
HERACLES: A HFO₂ FERROELECTRIC CAPACITOR COMPACT MODEL FOR EFFICIENT CIRCUIT SIMULATIONS

✉ Luca Fehlings^{*1}, ✉ Md Hanif Ali², ✉ Paolo Gibertini¹, ✉ Egidio A. Gallicchio¹, ✉ Udayan Ganguly², ✉ Veeresh Deshpande², and ✉ Erika Covi¹

¹Zernike Institute for Advanced Materials & Groningen Cognitive Systems and Materials Center (CogniGron)
University of Groningen, 9747 AG Groningen, Netherlands

²Department of Electrical Engineering, Indian Institute of Technology Bombay, Mumbai 400076, India

ABSTRACT

This paper presents a physics-based compact model for circuit simulations in a SPICE environment for HfO₂-based ferroelectric capacitors (FeCaps). The model has been calibrated based on experimental data obtained from HfO₂-based FeCaps. A thermal model with an accurate description of the device parasitics is included to derive precise device characteristics based on first principles. The model incorporates statistical data that enables Monte Carlo analysis based on realistic distributions, thereby making it particularly well-suited for design-technology co-optimization (DTCO). Furthermore, the model is demonstrated in circuit simulations using an integrated circuit with current programming, wherein partial switching of the ferroelectric polarization is observed. Finally, the model was benchmarked in an array simulation, reaching convergence in 1.8 s with an array size of 100 kb.

1 Introduction

Ferroelectric capacitors have the potential to be utilized in a multitude of applications that require a significant workload beyond that of memory storage [1]. The advent of new paradigms, such as in-memory and analog computing, necessitates the application of the DTCO methodology. The ability to integrate devices and circuits to reproduce sophisticated functionalities or accelerate computation while simultaneously optimizing power efficiency, density, and cost necessitates the development of compact models. It is imperative that these models accurately describe the behavior of the devices in question and that they converge reliably when used in conjunction with CMOS circuits in large arrays. In this context, it becomes important to conceive compact models that accurately describe not only the transient behavior of the FeCap but also consider parasitics and variability. This will enable circuit designers to test the robustness of their system with a realistic behavior of the devices. A variety of models have already been proposed, with a specific focus on the reproduction of particular behaviors [2, 3, 4, 5, 6, 7], such as DC operation, partial switching of the polarization, or Monte Carlo variations. However, a comprehensive model that could accurately describe all the behaviors exhibited by the FeCap is currently lacking.

In this work, we propose a physics-based compact model of FeCaps based on Hf_{0.5}Zr_{0.5}O₂ (HZO) which is validated on experimental data and includes a realistic distribution of the device-to-device variability. Furthermore, the model considers the intrinsic depletion of the electrodes and potential non-conductive or low-conductive interface layers, such as oxidized electrodes, and incorporates thermal modeling for both the polarization switching process and the leakage currents. The switching phenomenon then results from a complex process where the electric field experienced by the ferroelectric is affected by positive and negative feedback via the depletion and interface layer, leading to several characteristics observed in HfO₂-based ferroelectric devices. Subsequently, the model is employed in circuit simulations, wherein it is subjected to current programming pulses. To assess its performance, Monte Carlo simulations are conducted. Finally, the model is tested at an array level to investigate its computational load.

*Corresponding author: l.d.fehlings@rug.nl

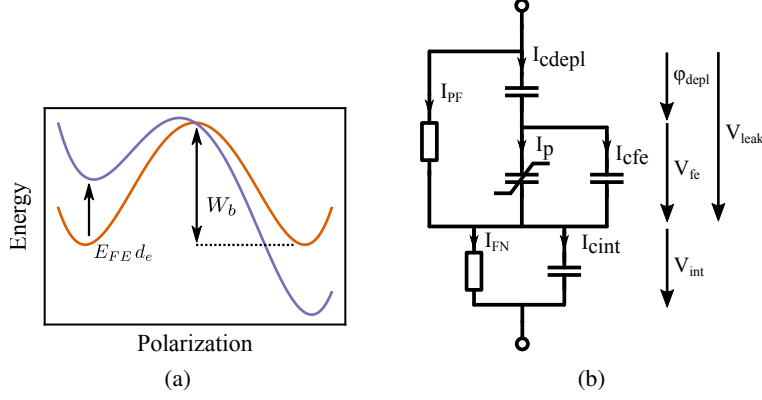


Figure 1: (a) Illustration of the energy profile based on Landau theory, where the ferroelectric switching process is modeled by a thermodynamic transition over the barrier W_b , modulated by the applied field (purple curve). (b) Equivalent circuit of the model, with internal nodes for the interface and depletion layers. The voltage applied to the device is then distributed between the branches by the spice simulation.

2 Physical device model

The compact model, available open source under the MIT license [8], is implemented in VerilogA and simulated using the Cadence Spectre SPICE simulator. An explanation of all parameters with their fitting values is listed in Tab. 1. In the model the intrinsic switching process is modeled by a non-equilibrium thermodynamic process where the transition rates $k_{\downarrow/\uparrow}$ are governed by a process with energy barrier W_b (Eq. 1), which is modulated by the electric field E_{fe} applied to the ferroelectric (Eq. 2), akin to the Landau free energy description of a ferroelectric (Fig. 1a). This results in the state variable p (Eq. 3) that describes the system's probability to be in the up polarization state. Assuming that this switching process (or nucleation) of an elementary site does not directly interact with other elementary sites, we can assume the proportion of domains in one of the polarization states to be equal to the occupation probability of that polarization state [9]. Accordingly, since p is a probability assuming values between 0 and 1, we can calculate the polarization change, equivalent to the polarization displacement current I_p , via Eq. 4.

$$k_{\downarrow/\uparrow} = \frac{k_B T}{h} \cdot \exp\left(\frac{(-W_b \pm W_e)}{k_B T}\right) \quad (1)$$

$$W_e = (E_{fr} - E_{off}) \cdot d_e \quad (2)$$

$$\frac{dp}{dt} = k_{\downarrow}(1 - p) - k_{\uparrow}p \quad (3)$$

$$I_p = \frac{dP}{dt} = \frac{d(2P_s p)}{dt} \quad (4)$$

Macroscopically, however, there is an interaction between these elementary sites, as the depolarization field acts as a feedback mechanism that modulates the electric field in the switching process proportional to the device polarization. Hence, an accurate description of the switching behavior needs to consider this depolarization field, which we model via an interface layer capacitance C_{int} (Eq. 7), and leakage current I_{FN} (Eq. 10) and an intrinsic depletion capacitance of the electrodes C_{depl} (Eq. 5), which is non-negligible due to the high displacement and thus charge density at the electrode interfaces [10]. The structure of the model elements is depicted in the equivalent circuit (Fig. 1b).

$$C_{depl} = p \cdot C_{depl\downarrow} + (1 - p) \cdot C_{depl\uparrow} \quad (5)$$

$$C_{depl\downarrow/\uparrow} = \frac{\varepsilon_{depl} q N_{depl\downarrow/\uparrow}}{\varepsilon_{fe} E_{fe} \pm Q_{fix,depl}} \quad (6)$$

$$C_{fe/int} = \frac{\varepsilon_0 \varepsilon_{fe/int}}{t_{fe/int}} \quad (7)$$

The voltage V_{fe} experienced by the ferroelectric layer then depends on the voltage drop over the interface layer V_{int} and the depletion capacitance ε_{depl} , which sums up to the total applied voltage V_{app} (Eq. 9). A depolarization field then

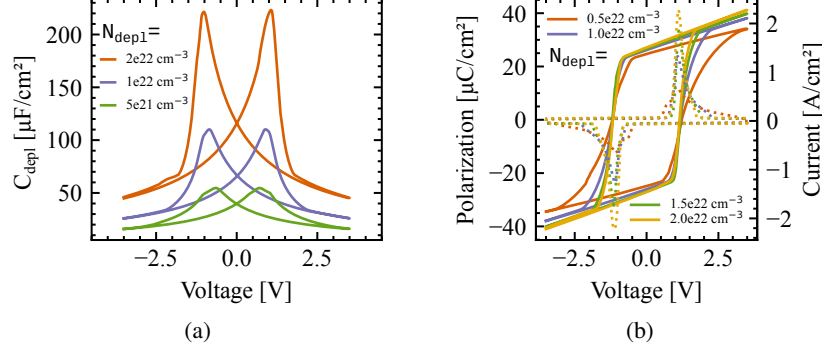


Figure 2: (a) Simulated small signal capacitance C_{depl} , a part of the total MFM capacitance (cf. Fig. 4a), for different carrier densities in the depletion layer. A hysteresis is observed due to the independent modeling of the depletion layers for each polarization direction. (b) Simulated polarization hysteresis at 1 kHz for decreasing carrier densities in the depletion layer, where both the remanent polarization as well as the switching peak sharpness decrease as the carrier density in the electrode decreases. The dotted lines show the respective displacement currents.

arises from the charges originating from the ferroelectric switching process which lead to a voltage over the interface and depletion capacitances.

$$\varphi_{depl} = \frac{2P_s p - P_s + C_{fe} V_{fe}}{C_{depl}} \quad (8)$$

$$V_{appl} = V_{fe} + V_{int} + \varphi_{depl} \quad (9)$$

The depletion capacitance (Eq. 5, Fig. 2a), which we model independently for both polarization directions [11] similar to the polysilicon depletion model (Eq. 6) [12], in particular has a pronounced influence on the switching process, as it severely slows down the switching process (Fig. 2b) due to the low series capacitance. This phenomenon can be severely impacted by charge screening due to trapped charges, which is modeled by the static charge $Q_{fix,depl}$, which we expect to be related to the saturation polarization P_s of the ferroelectric layer. In addition, we consider the leakage current through the interface layer and the ferroelectric layer via Fowler-Nordheim (Eq. 10) and Poole-Frenkel (Eq. 11) conduction mechanisms respectively.

$$J_{FN} = \frac{q^3}{8\pi\hbar q\phi_{b,int}} E_{int}^2 \exp\left(-\frac{8\pi\sqrt{2m_0 m_{eff,int}}(q\phi_{b,int})^{3/2}}{3\hbar q E_{int}}\right) \quad (10)$$

$$J_{PF} = q\mu_{fe} N_{fe} E_{leak} \exp\left[\frac{-q\left(\phi_{tr,fe} - \sqrt{\frac{qE_{leak}}{\pi\varepsilon_0\varepsilon_{fe}}}\right)}{kT}\right] \quad (11)$$

As a result, the compact model is applicable in several circuit simulation procedures, such as DC, AC, or transient simulations under arbitrary voltage or current waveforms.

3 Experimental validation

Based on experimental data on switching kinetics (Fig. 3a), obtained from a HZO FeCap (Fig. 3b), we verified the transient switching process of the model, and obtained the parameters listed in Tab. 1. The fabrication details are described elsewhere [13], and all experimental measurements are performed after 1000 wake-up cycles at 3 V, unless otherwise noted.

Using the extracted set of parameters, we compared the experimental hysteresis curve of a device after wake-up with the simulation (Fig. 3c) and obtained a close match. Further, the model also provides a capacitance hysteresis that resembles the characteristic butterfly shape (Fig. 4a), which also reflects the voltage bias seen in the polarization hysteresis, and models the leakage current through the device (Fig. 4b) with independent contributions from both the HZO layer as well the interface layer. The model also replicates the hysteresis loop at lower voltages (Fig. 5a) and, with parameters adjusted for oxidation or degradation of the electrodes, lowering the depletion capacitance, is further able to model the

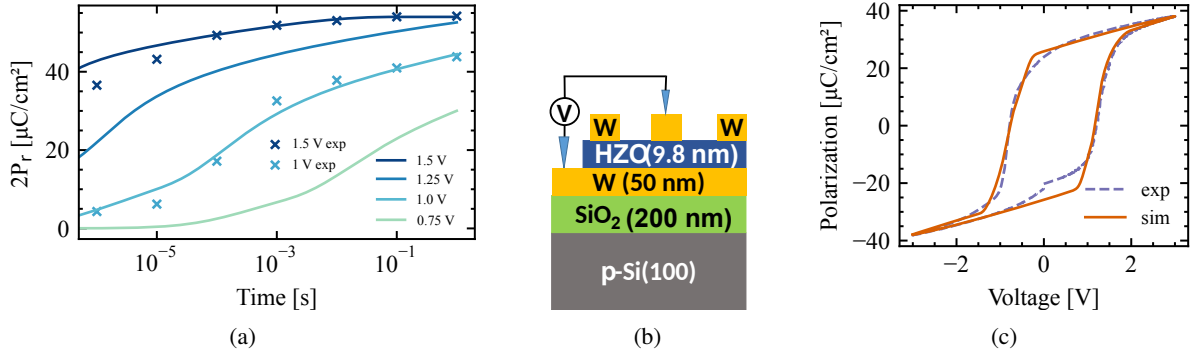


Figure 3: (a) Switching kinetics of the device, simulated using the parameters in Tab. 1., and experimental data used for the parameter extraction. (b) Material stack of the MFM device from which the experimental data was gathered. (c) Hysteresis loop at 1 kHz for a woken-up device, resulting from the same parameters, showing that model generalizes the switching process well.

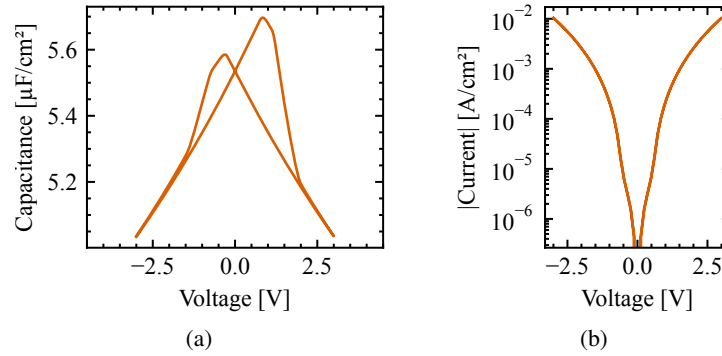


Figure 4: (a) Simulated small signal capacitance of the MFM stack, highlighting the influence of the depletion capacitance (Fig. 2a). Notably the offset field E_{off} also leads to an asymmetry in the capacitance hysteresis. (b) DC simulation of the current, resulting from the Poole-Frenkel current for the ferroelectric layer in series for the Fowler-Nordheim current for the interface layer.

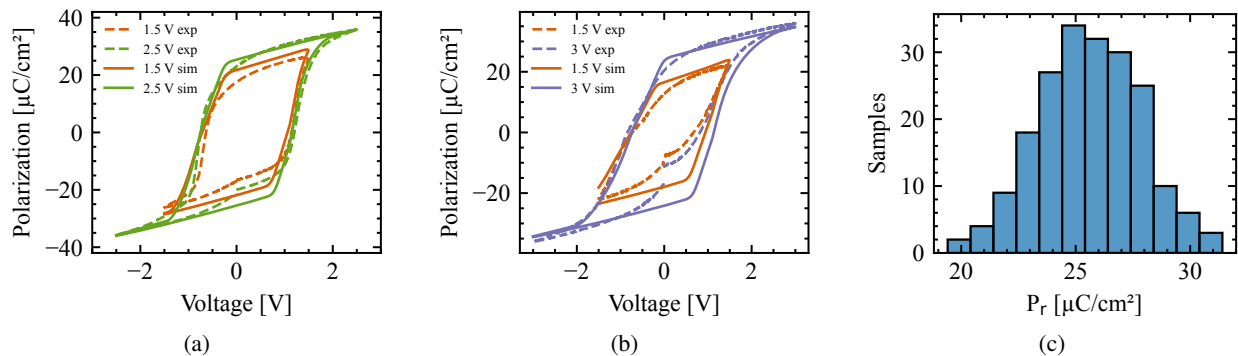


Figure 5: (a) Hysteresis at low voltages and 1 kHz frequency that do not saturate the polarization and have a lower apparent coercive field due to the increased voltage ramp rate. (b) Hysteresis of a pristine device for different voltages, obtained by adjusting N_{depl} to $7e21 \text{ cm}^{-3}$, highlighting the increase of carrier density at the electrode interface as a possible contribution to the wake-up mechanism. (c) Histogram of the remanent polarization obtained from a Monte Carlo simulation of the 1 kHz hysteresis.

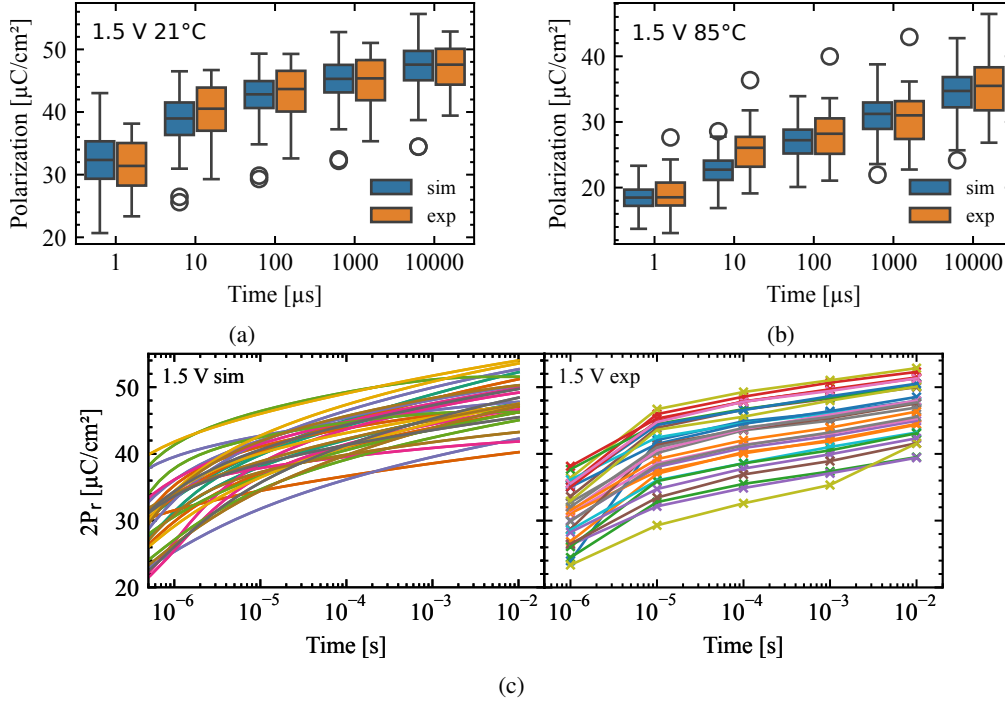


Figure 6: (a) Variability of the switched polarization at 21 °C in the experiment and in the Monte Carlo simulation. (b) Switched polarization at 85 °C, due to the elevated temperatures the polarization screening was modeled by a decrease in d_e and an increase in $Q_{fix,depl}$ to account for increased charge trapping. (c) Direct comparison of the switching transients of the Monte Carlo simulation and the experimental data at 1.5 V and 21 °C.

polarization hysteresis of the pristine device (Fig. 5b), suggesting that the depletion capacitance is a plausible factor in the wake-up process.

As a further step towards application in circuit design and DTCO methods, the model is validated against an experimental variability study of the switching kinetics with Monte Carlo simulations (Fig. 6a). The parameters used to model the variability (Tab. II), while not an exhaustive description of all possible variability sources, can approximate the experimental variability also in the individual polarization transients (Fig. 6c). Based on these parameters, the influence on the remanent polarization (Fig. 5c) is also evident. A further comparison was carried out on experimental switching kinetics at 85 °C (Fig. 6b) where, with a parameter adjustment accounting for an increase in interface charges due to charge (de-)trapping at high temperatures, the Monte Carlo simulation based on the thermal model also predicts both the switched polarization as well as the increasing spread of the polarization for longer time frames.

4 Circuit simulation

The availability of a stable compact model allows the exploration of new device applications that are hard to verify using standard test equipment such as semiconductor parameter analyzers and without a monolithic co-integration of FeCaps and CMOS circuits. One such case of study is the behavior of a FeCap programmed using a current source. Here, the model is employed in a current programming circuit (Fig. 7a). A current pulse is fed to the FeCap using two transistors in saturation, with two control transistors that either source or sink current. A train of 250 nA high and 10 μs wide current pulses is then applied to the FeCap, which is fully discharged to 0 V after each pulse. The train of pulses is then compared with a single 1 ms pulse of 25 nA, the average current of the train of pulses.

The Monte Carlo simulation (Fig. 7b) shows the evolution of the polarization with the current pulses, including the standard deviation. The model can achieve partial polarization switching, an important feature in applications that require analog computing or multilevel programming. Furthermore, it can predict the polarization switched by current input pulses, differentiating between different stimulating pulses. Accordingly, the model is able to assist the design of reliable FeCap-based circuits robust to device variation. Additionally, the model was tested in a 30 μs transient programming simulation using arrays of different sizes (Fig. 7c), reaching convergence in 1.8 s with an array size of 100 kb.

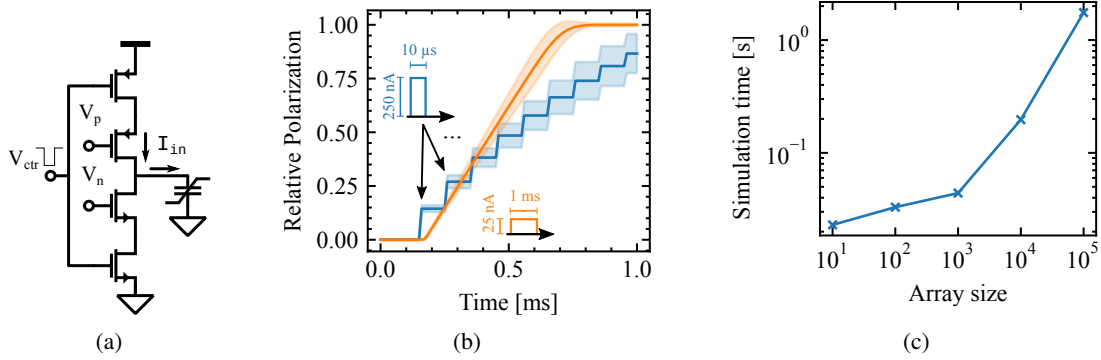


Figure 7: (a) Current programming circuit, with two transistors in saturation acting as current source and sink. (b) Simulation of a $25 \mu\text{m}^2$ FeCap programmed with a train of current pulses and a single pulse using the current programming circuit. The shaded area is the standard deviation obtained from the Monte Carlo simulation. (c) Simulation time, as a function of the array size, for a transient simulation of a single current pulse applied using the circuit the current programming circuit.

5 Conclusion

We developed a compact model of HZO FeCap, implemented in VerilogA and open source under the MIT license, with the specific objective of enabling circuit simulations for DTCO and eventually system-technology co-optimization (STCO). The model employs a comprehensive physics-based approach that accounts for a range of factors, including interface parasitic capacitances, leakage current, thermal effects, partial polarization switching, and device-to-device variations. The model has been calibrated using experimental data from several devices and enables Monte Carlo simulations based on a realistic distribution. The functionality of the model is demonstrated in circuit simulation using a current programming circuit at both the single-device and array levels. Despite the inclusion of several complex physical effects, the model converges and runs at a reasonable time for large device numbers, and for a wide range of parameters in Monte Carlo simulations, indicating its readiness for practical circuit design.

Acknowledgments

The Authors thank Dr. Fernando M. Quintana for the fruitful discussions. This work was supported by the European Research Council (ERC) through the European’s Union Horizon Europe Research and Innovation Programme under Grant Agreement No 101042585. Views and opinions expressed are however those of the authors only and do not necessarily reflect those of the European Union or the European Research Council. Neither the European Union nor the granting authority can be held responsible for them. The Authors would like to acknowledge the financial support of the CogniGron research center and the Ubbo Emmius Funds (Univ. of Groningen). IIT Bombay acknowledges funding from DST and MeitY through the NNETRA project of Govt. of India.

References

- [1] N. Ramaswamy, A. Calderoni, J. Zahurak, G. Servalli, A. Chavan, S. Chhajed, M. Balakrishnan, M. Fischer, M. Hollander, D. P. Ettisserry, A. Liao, K. Karda, M. Jerry, M. Mariani, A. Visconti, B. R. Cook, B. D. Cook, D. Mills, A. Torsi, C. Mouli, E. Byers, M. Helm, S. Pawlowski, S. Shiratake, and N. Chandrasekaran, “Nvdram: A 32gb dual layer 3d stacked non-volatile ferroelectric memory with near-dram performance for demanding ai workloads,” in *2023 International Electron Devices Meeting (IEDM)*, pp. 1–4, 2023.
- [2] M. Pešić, C. Künneth, M. Hoffmann, H. Mulaosmanovic, S. Müller, E. T. Breyer, U. Schroeder, A. Kersch, T. Mikolajick, and S. Slesazek, “A computational study of hafnia-based ferroelectric memories: from ab initio via physical modeling to circuit models of ferroelectric device,” *Journal of computational electronics*, vol. 16, pp. 1236–1256, 8 2017.
- [3] C. Alessandri, P. Pandey, and A. C. Seabaugh, “Experimentally validated, predictive monte carlo modeling of ferroelectric dynamics and variability,” in *2018 IEEE International Electron Devices Meeting (IEDM)*, pp. 16.2.1–16.2.4, 2018.
- [4] T. Kim, J. A. del Alamo, and D. A. Antoniadis, “Dynamics of HfZrO_2 Ferroelectric Structures: Experiments and Models,” in *2020 IEEE International Electron Devices Meeting (IEDM)*, pp. 21.4.1–21.4.4, 2020.
- [5] C.-T. Tung, G. Pahwa, S. Salahuddin, and C. Hu, “A compact model of polycrystalline ferroelectric capacitor,” *I.E.E.E. transactions on electron devices/IEEE transactions on electron devices*, vol. 68, pp. 5311–5314, 10 2021.
- [6] N. Feng, H. Li, C. Su, L. Zhang, R. Huang, Qianqian andegidio angelo gallicchio Wang, and R. Huang, “A dynamic compact model for ferroelectric capacitance,” *IEEE electron device letters*, vol. 43, pp. 390–393, 3 2022.

- [7] Z.-Y. Yan, R. Zhao, Z. Wang, T. Lu, H. Liu, K.-H. Xue, X. Miao, Y. Yang, and T.-L. Ren, "A Liouville Model for Polycrystalline Ferroelectrics Emphasizing Kinetic Integrity and Deployability in Circuits with Charge and Current Constraints," in *2023 International Electron Devices Meeting (IEDM)*, 12 2023.
- [8] L. Fehlings, P. Gibertini, E. A. Gallicchio, and E. Covi, "bics-rug/heracles: v0.1.0," Sept. 2024.
- [9] M. Vopsaroiu, J. Blackburn, M. G. Cain, and P. M. Weaver, "Thermally activated switching kinetics in second-order phase transition ferroelectrics," *Phys. Rev. B*, vol. 82, p. 024109, Jul 2010.
- [10] C. Black and J. Welser, "Electric-field penetration into metals: consequences for high-dielectric-constant capacitors," *IEEE Transactions on Electron Devices*, vol. 46, no. 4, pp. 776–780, 1999.
- [11] T. Kim, E. R. Borujeny, I. Sardinero-Meirás, J. Grajal, K. C. Cadien, D. A. Antoniadis, and J. A. Del Alamo, "Ac impedance characteristics of ferroelectric hf0.5zr0.5o2: from 1 khz to 10 ghz," in *2023 International Electron Devices Meeting (IEDM)*, pp. 1–4, 2023.
- [12] N. Arora, E. Rios, and C.-L. Huang, "Modeling the polysilicon depletion effect and its impact on submicrometer cmos circuit performance," *IEEE Transactions on Electron Devices*, vol. 42, no. 5, pp. 935–943, 1995.
- [13] M. H. Ali, A. Pandey, S. Shirodkar, R. Srinu, P. Meihar, U. Ganguly, and V. Deshpande, "Enhanced polarization, endurance, and long retention in low temperature processed w/hf0.5zr0.5o2/w ferroelectric capacitor for back-end-of-line integration," in *2024 8th IEEE Electron Devices Technology & Manufacturing Conference (EDTM)*, pp. 1–3, 2024.

Appendix: Parameters and constants

Parameter	Value	Unit	Description
A	625	μm^2	Device area
t_{fe}	9.8	nm	Ferroelectric layer thickness
t_{int}	1	nm	Interface layer thickness
ε_{fe}	70	1	HZO relative permittivity
ε_{int}	90	1	Interface layer relative permittivity
ε_{depl}	3.6	1	Polarizability of depletion layer
W_b	1.05	eV	Switching energy barrier
d_e	7.5	nm	Electric field action distance
E_{off}	0.2	MV/cm	Internal bias electric field
P_s	27	$\mu\text{C}/\text{cm}^2$	Saturation polarization density
N_{depl}	$1.4 \cdot 10^{22}$	cm^{-3}	Carrier density in depletion layer
N_{fe}	$1 \cdot 10^{18}$	cm^{-3}	Conduction band density of states
$Q_{fix,depl}$	9.45	$\mu\text{C}/\text{cm}^2$	Fixed charge at the depletion interface
$m_{eff,int}$	1	1	Electron effective mass in the interface
$\phi_{b,int}$	0.65	V	Electrode/interface barrier height
$\phi_{tr,fe}$	0.68	V	Conduction band trap depth in HZO
μ_{fe}	$15 \cdot 10^{-4}$	$\text{m}^2\text{V}^{-1}\text{s}^{-1}$	Charge carrier mobility in HZO

Table 1: FeCap model parameters as obtained from the parameter extraction on the switching kinetics 3a and polarization hysteresis 3c measurements.

Parameter	μ @ 21°C	μ @ 85°C	σ
t_{int}	1.5 nm	1.5 nm	0.22 nm
P_s	27 $\mu\text{C}/\text{cm}^2$	27 $\mu\text{C}/\text{cm}^2$	2.7 $\mu\text{C}/\text{cm}^2$
N_{depl}	$1.05 \cdot 10^{22} \text{cm}^{-3}$	$1.05 \cdot 10^{22} \text{cm}^{-3}$	$2.65 \cdot 10^{21} \text{cm}^{-3}$
$Q_{fix,depl}$	9.8 $\mu\text{C}/\text{cm}^2$	27 $\mu\text{C}/\text{cm}^2$	0
d_e	7.5 nm	4.5 nm	0

Table 2: Monte Carlo parameters, with mean value μ and standard deviation σ , as extracted from the switching kinetics measurements at 21 °C (Fig. 6a) and 85 °C 6b.

Parameter	Description
k_B	Boltzmann constant
h	Planck constant
q	Elementary charge
ε_0	Vacuum permittivity
m_0	Electron rest mass

Table 3: Physical constants used in the equations